

Microstructures and Thermoelectric Properties of Sintered $\text{Ca}_3\text{Co}_4\text{O}_9$ -based oxide.

Takao Morimura,^{1,2} Masayuki Hasaka,¹ Shin-ichiro Kondo,¹ Hiromichi Nakashima,¹ Hisamitsu Maeda

1. —Graduate School of Engineering, Nagasaki University, 1-14 Bunkyo-machi, Nagasaki 852-8521, Japan. 2.—e-mail: tmori@nagasaki-u.ac.jp

Abstract

Zn- and Ti- doped thermoelectric misfit cobalt oxides $\text{Ca}_3\text{Co}_{4-x-y}\text{Zn}_x\text{Ti}_y\text{O}_9$ ($x = 0 - 0.5$, $y = 0 - 0.5$) were prepared by solid-phase reaction, sequent uniaxial compression molding and sintering at 1173 K for 20 h. Powder X-ray diffraction data suggest that Zn and Ti dopants substitute in the rocksalt layer rather than in the CoO_2 layer for $x \leq 0.1$ and $y \leq 0.1$, respectively. In Zn and Ti single-doped samples for $x \leq 0.1$ and $y \leq 0.1$, ZT at room temperature increased with x and y through an increase in the absolute Seebeck coefficients despite the decrease in electrical conductivities. In Zn and Ti double-doped samples, minor phases other than the misfit oxides were observed at approximately $x + y \geq 0.1$. At $x \leq 0.1$ and $y \leq 0.1$ double doping improved the thermoelectric properties. ZT at room temperature reached a maximum value of 0.035 at $(x, y) = (0.1, 0.03)$.

Key words: Seebeck coefficient, dimensionless figure of merit, XRD-Rietveld method, high resolution TEM, Harman method

Introduction

The misfit cobalt oxides $\text{Ca}_3\text{Co}_4\text{O}_9$ are good representatives of thermoelectric materials because of the high dimensionless figure of merit ZT and superior thermal stability at high temperatures. $\text{Ca}_3\text{Co}_4\text{O}_9$ is monoclinic and consists of alternate stacks of a triple rocksalt Ca_2CoO_3 layer (RS) and a CdI_2 -

type CoO_2 layer along the c -axis. The two types of layers have the same a , c and β lattice parameters but different b_{CoO_2} and b_{RS} parameters^(1,2). The CoO_2 and rocksalt layers are considered responsible for the electrical and thermal properties, respectively. The thermoelectric properties strongly depend on atomic substitution by dopants⁽³⁻¹⁰⁾. Investigations of atomic substitutions are important for improving the thermoelectric performance. It was reported that the substitution of Co by transition metals strongly improves ZT ⁽¹¹⁻¹²⁾. In particular, the substitution by Zn and Ti is possible because of the proximity in the ionic radii of Zn, Ti and Co⁽¹³⁾.

In the present study, single- and double-doped misfit cobalt oxides $\text{Ca}_3\text{Co}_{4-x-y}\text{Zn}_x\text{Ti}_y\text{O}_9$ ($x = 0 - 0.5$, $y = 0 - 0.5$) were fabricated by solid-phase reaction, sequent uniaxial compression molding and sintering at 1173 K for 20 h. The effect of Zn and Ti doping on the microstructures and thermoelectric properties was investigated by powder X-ray diffraction (XRD), high-resolution transmission electron microscopy (TEM) and by measuring the Seebeck coefficient, electrical conductivity and dimensionless figures of merit.

Experimental procedure

CaCO_3 , Co_3O_4 , ZnO and TiO_2 powders were weighed according to the proportions of the $\text{Ca}_3\text{Co}_{4-x-y}\text{Zn}_x\text{Ti}_y\text{O}_9$ composition ($x = 0 - 0.5$, $y = 0 - 0.5$). The powders were thoroughly mixed with acetone in an agate mortar, heated at 1123 K for 20 h in an alumina crucible in air and then slowly cooled to room temperature. The products were ground into powder ($\sim 75 \mu\text{m}$), molded in uniaxial compression at 900 MPa and then sintered at 1173 K for 20 h in air to fabricate pellet samples having 10.4 mm diameter and 1.3 mm thickness.

The Seebeck coefficient α was determined by measuring the voltage at both ends of the pellets, which is caused by the difference in temperature. Electrical conductivity σ was measured using the four-point probe method at room temperature. The dimensionless figure of merit ZT was measured by the Harman method⁽¹⁴⁾ at room temperature. For the XRD samples, the pellets were ground into powder

(~75 μm). The XRD patterns were obtained by using a Rigaku Rint-2200VL and Cu K_{α} radiation. The patterns were analyzed by the Rietveld method using the RIETAN code⁽¹⁵⁾. TEM observations of the microstructures were performed using a JEOL JEM-2010 at the Joint Research Center, Nagasaki University.

Results and Discussion

Figures 1 (a) and (b) show the powder X-ray diffraction patterns of the single-doped misfit cobalt oxides $\text{Ca}_3\text{Co}_{4-x-y}\text{Zn}_x\text{Ti}_y\text{O}_9$ ($x = 0 - 0.5$, $y = 0$) and ($x = 0$, $y = 0 - 0.5$), respectively. Most diffraction peaks are indexed as the misfit cobalt oxide $\text{Ca}_3\text{Co}_4\text{O}_9$ phase although weak peaks of $\text{Ca}_3\text{Co}_2\text{O}_6$ and ZnO phases are observed for $x > 0.1$ in (a), and weak unknown peaks are observed for $y > 0.1$ in (b), as indicated by the arrows. These peak intensities increased with x and y . The solution limits are considered to be around $x=0.1$ and $y=0.1$.

Figures 2 (a) and (b) show the lattice constants a (\circ), c (\blacktriangle), b_{RS} (\circ) and b_{CoO_2} (\blacktriangle) in the Zn single-doped sample ($y = 0$) as a function of x . The lattice constants were determined using Rietveld analysis in the range of $15^\circ - 80^\circ$ (Fig. 1). Lattice constants a , c and b_{RS} seem to decrease with increasing x , whereas b_{CoO_2} is almost constant as x changes. Figures 3 (a) and (b) show the lattice parameters a , c , b_{RS} and b_{CoO_2} of the Ti single-doped sample ($x = 0$) as a function of y . In Fig. 3 (a), c slightly decreases with increasing y although a is nearly constant. In Fig. 3 (b), b_{CoO_2} is nearly constant as y changes, whereas b_{RS} decreases with increasing y . These results suggest that Zn and Ti substitute in the rocksalt layer rather than in the CoO_2 layer.

The density of the sintered pellet for $x = y = 0$ was measured to be 3.98 g/cm^3 by the Archimedes method. Compared with the density estimated from the lattice constants measured by the present XRD measurements and the atomic weights, the relative density was estimated to be 77.6 %.

Bright-field TEM images indicate that the crystal grain size is about $1 \mu\text{m}$. Figure 4 shows a high-resolution TEM image and the diffraction pattern of $\text{Ca}_3\text{Co}_{3.9}\text{Zn}_{0.1}\text{O}_9$ in the $[\bar{1}010]$ incident direction.

The indices in the diffraction pattern and the incident direction were defined by the four-dimensional superspace group approach⁽²⁾. From the comparison of Fig. 4 with the simulated image, the CaO and CoO planes in the rocksalt layer and the CoO₂ layer were confirmed as indicated by the inset projection.

Figures 5 (a) and (b) show the Seebeck coefficient α (\circ) measured at 473 K, the electrical conductivity σ (\blacktriangle) and dimensionless figure of merit ZT (\circ) at room temperature in a Zn single-doped sample ($y = 0$) as a function of x . The Seebeck coefficients were positive, indicating p-type conductivity. ZT increases with x through the increase in α despite the decrease in σ . The increase in ZT with x is attributed to the decrease in thermal conductivity κ because of the substitution in the rocksalt layer by Zn. ZT reaches a maximum at $x = 0.1$ near the solution limit. Figures 6 (a) and (b) show α (\circ), σ (\blacktriangle) and ZT (\circ) of the Ti single-doped sample ($x = 0$) as a function of y . In analogy with Fig. 5, ZT increases with y through the slight increase in α regardless of the decrease in σ . The increase in ZT with x is attributed to the decrease in κ because of the substitution in the rocksalt layer by Ti. Similar results were reported in a previous paper for a Ti single-doped sample, measured between 300 K and 1000 K⁽⁷⁾, which confirms the present results at room temperature. Clearly, the present results show that single doping of Zn or Ti effectively improves of the thermoelectric properties.

The rocksalt layer includes Co³⁺⁽¹⁶⁾, which is partially substituted by Ti⁴⁺⁽¹⁷⁾. The substitution decreases the valence of Co in the CoO₂ layer because of the charge conservation rule and may increase the Seebeck coefficient according to the extended Heikes formula⁽¹⁸⁾. This mechanism reasonably explains the present results for the Ti single-doped sample. However, this is not the case in the Zn single-doped sample because Zn ion is bivalent. Therefore, more experiments regarding the Zn occupancy are required for the Zn single-doped sample.

The X-ray diffraction patterns of the Zn and Ti double-doped samples were measured for $0 \leq x \leq 0.1$ and $0 \leq y \leq 0.1$. The sample compositions and XRD results are plotted in Fig. 7. When $x + y$ was large, minor phases other than the misfit cobalt oxide were observed. Single-phase misfit cobalt oxide Ca₃Co₄O₉ sample (\circ), and the sample containing few minor phases (Δ) and many minor phases (\square) were

clarified by X-ray diffraction as shown in Fig. 7. The approximate solution limit is shown as the broken curve in Fig. 7.

The thermoelectric properties were measured for the sample plotted in Fig. 7. The measurements of α , σ and ZT were plotted as a function of x and y , and the thermoelectric property maps were also drawn (Fig. 8). The brightness in the maps is proportional to the actual measured values. The high performance areas are clarified in the maps although the contours of the maps are not smooth because of the small number of data. For the Seebeck coefficient (a), double doping is effective; it increases with x and y but decreases in the high Ti content area. The maximum 220 $\mu\text{V/K}$ is obtained at $(x, y) = (0.1, 0.03)$. For the electric conductivity (b), double doping is not effective; it decreases with increasing x and y , and a minimum is obtained at $(x, y) = (0.05, 0.08)$. For ZT , double doping is effective and a maximum of 0.035 is obtained at $(x, y) = (0.1, 0.03)$ through the increase in α despite the decrease in σ .

Conclusions

Zn- and Ti-doped misfit cobalt oxides $\text{Ca}_3\text{Co}_{4-x-y}\text{Zn}_x\text{Ti}_y\text{O}_9$ ($x = 0 - 0.1$, $y = 0 - 0.1$) were prepared by solid-phase reaction, sequent uniaxial compression molding and sintering at 1173 K for 20 h. XRD analysis of Zn single-doped samples ($y = 0$) showed minor phases of $\text{Ca}_3\text{Co}_2\text{O}_6$ and ZnO in addition to the major phase of misfit oxide $\text{Ca}_3\text{Co}_4\text{O}_9$ for $x \geq 0.1$. In Ti single-doped samples ($x = 0$), a minor unknown phase other than the misfit cobalt oxide was observed for $y \geq 0.1$. In both the Zn and Ti single-doped samples, the lattice constant b_{RS} decreased with increasing x and y , respectively, whereas b_{CoO_2} was nearly constant. This suggests that the Zn and Ti dopants substitute in the rocksalt layer rather than in the CoO_2 layer. In both single-doped samples for $x \leq 0.1$ and $y \leq 0.1$, ZT at room temperature increased with x and y through an increase in the absolute Seebeck coefficients despite the decrease in electrical conductivities. In the Zn and Ti double-doped samples, minor phases other than the misfit oxides were observed approximately at $x + y \geq 0.1$. It is seen that for $x \leq 0.1$ and $y \leq 0.1$ double doping

was significantly effective in improving the thermoelectric properties. ZT at room temperature reached a maximum value of 0.035 at $(x, y) = (0.1, 0.03)$ through the increase in α despite the decrease in σ .

Acknowledgements

This work was partially supported by ‘Grant-in-Aid for Scientific Research (No. 21560687)’ from the Japan Society for the Promotion of Science (JSPS).

References

1. A.C. Masset, C. Michel, A. Maignan, M. Hervieu, O. Toulemonde, F. Studer, B. Raveau, *Phys. Rev. B* 62, 166 (2000).
2. Y. Miyazaki, K. Kudo, M. Akoshima, Y. Ono, Y. Koike, T. Kajitani, *Jpn. J. Appl. Phys.* 39, L531 (2000).
3. D. Wang, L. Chen, Q. Yao, J. Li, *Solid State Commun.* 129, 615 (2004).
4. M. Prevel, O. Perez, J.G. Noudem, *Solid State Sci.* 9, 231 (2007).
5. Y. Wang, Y. Sui, J. Cheng, X. Wang, J. Miao, Z. Liu, Z. Qian, W. Su, *J. Alloys Compd.* 448, 1 (2008).
6. G. Tang, C. Tang, X. Xu, Y. He, L. Qiu, L. Lv, Z. Wang, Y. Du, *Solid State Commun.* 150, 1706 (2010).
7. L. Xu, F. Li, Y. Wang, *J. Alloys Compd.* 501, 115 (2010).
8. N.V. Nong, C.-J. Liu, M. Ohtaki, *J. Alloys Compd.* 491, 53 (2010).
9. H.B. Yahida, F. Mauvy, J.C. Grenier, *J. Solid State Chem.* 183, 527 (2010).
10. J. Pei, G. Chen, N. Zhou, D.Q. Lu, F. Xiao, *Physica B* 406, 571 (2011).
11. Y. Wang, Y. Sui, P. Ren, L. Wang, X. J. Wang, W. H. Su, H. J. Fan, *Chem. Mater.* 22, 1155 (2010).
12. Y. Wang, Y. Sui, X. Wang, W. Sui, X. Liu, *J. Appl. Phys.* 107, 33708 (2010).
13. R. D. Shannon, *Acta Cryst. A* 32, 751 (1976).

14. R. Venkatasubramanian, E. Siivola, T. Colpitts and B. O'Quinn, *Nature* 413, 597 (2001).
15. F. Izumi and T. Ikeda, *Mater. Sci. Forum* 321-324, 198 (2000).
16. G. Yang, Q. Ramasse, R. F. Klie, *Phys. Rev. B* 78, 153109 (2008).
17. C. D. Ling, K. Aivazian, S. Schmid, P. Jensen, *J. Solid State Chem.* 180, 1446 (2007).
18. W. Koshibae, K. Tsutsui, S. Maekawa, *Phys. Rev. B* 62, 6869 (2000).

Figure captions

Fig. 1. Powder X-ray diffraction patterns for Zn or Ti single-doped samples of $\text{Ca}_3\text{Co}_{4-x-y}\text{Zn}_x\text{Ti}_y\text{O}_9$ ($x = 0 - 0.5$, $y = 0$) (a) and ($x = 0$, $y = 0 - 0.5$) (b). Minor phases other than the misfit oxide $\text{Ca}_3\text{Co}_4\text{O}_9$ are indicated by arrows.

Fig. 2. Lattice constants a (\circ) and c (\blacktriangle) (a), and b_{RS} (\circ) and b_{CoO_2} (\blacktriangle) (b) of Zn single-doped misfit cobalt oxides $\text{Ca}_3\text{Co}_{4-x-y}\text{Zn}_x\text{Ti}_y\text{O}_9$ ($y = 0$) as function of x . The lattice constants were determined using Rietveld analysis in the range of $15^\circ - 80^\circ$.

Fig. 3. Lattice constants a (\circ) and c (\blacktriangle) (a), and b_{RS} (\circ) and b_{CoO_2} (\blacktriangle) (b) of Ti single-doped misfit cobalt oxides $\text{Ca}_3\text{Co}_{4-x-y}\text{Zn}_x\text{Ti}_y\text{O}_9$ ($x = 0$) as function of y . The lattice constants were determined using Rietveld analysis in the range of $15^\circ - 80^\circ$.

Fig. 4. High-resolution TEM image and diffraction pattern of $\text{Ca}_3\text{Co}_{3.9}\text{Zn}_{0.1}\text{O}_9$ in the $[\bar{1}010]$ incident direction. The indices are defined by the four-dimensional superspace group approach.

Fig. 5. Seebeck coefficient α (\circ) measured at 473 K and the electrical conductivity σ (\blacktriangle) (a), and dimensionless figure of merit ZT (\circ) at room temperature (b) for the Zn single doped-misfit cobalt oxides $\text{Ca}_3\text{Co}_{4-x-y}\text{Zn}_x\text{Ti}_y\text{O}_9$ ($x = 0 - 0.1$, $y = 0$). Seebeck coefficients were positive and indicate p-type conductivity.

Fig. 6. Seebeck coefficient α (\circ) measured at 473 K and the electrical conductivity σ (\blacktriangle) (a), and dimensionless figure of merit ZT (\circ) at room temperature (b) for the Ti single-doped misfit cobalt oxides

$\text{Ca}_3\text{Co}_{4-x-y}\text{Zn}_x\text{Ti}_y\text{O}_9$ ($x = 0, y = 0 - 0.1$). Seebeck coefficients were positive and indicate p-type conductivity.

Fig. 7. Sample compositions of the double-doped misfit cobalt oxides $\text{Ca}_3\text{Co}_{4-x-y}\text{Zn}_x\text{Ti}_y\text{O}_9$ for $0 \leq x \leq 0.1$ and $0 \leq y \leq 0.1$. The single-phase sample of the misfit cobalt oxide phase (\circ), and the sample containing few minor phases (Δ) and many minor phases (\square) were clarified using the X-ray diffraction patterns.

Fig. 8. Maps of the Seebeck coefficient α (a) measured at 473 K, electrical conductivity σ (b) and dimensionless figure of merit ZT (c) at room temperature as a function of x and y for double-doped misfit cobalt oxides $\text{Ca}_3\text{Co}_{4-x-y}\text{Zn}_x\text{Ti}_y\text{O}_9$.

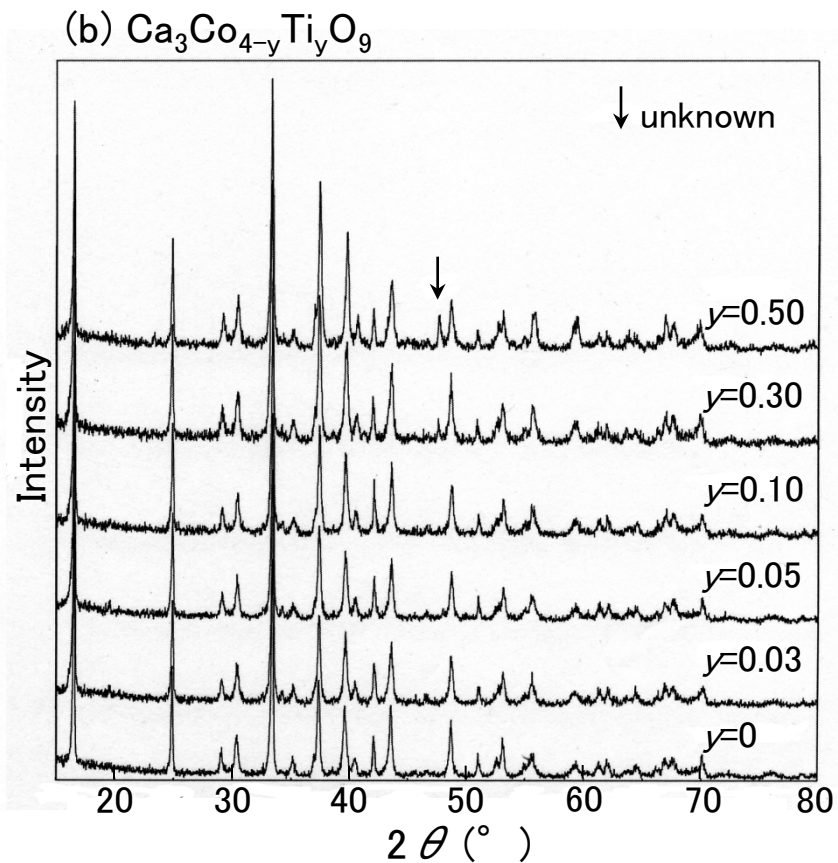
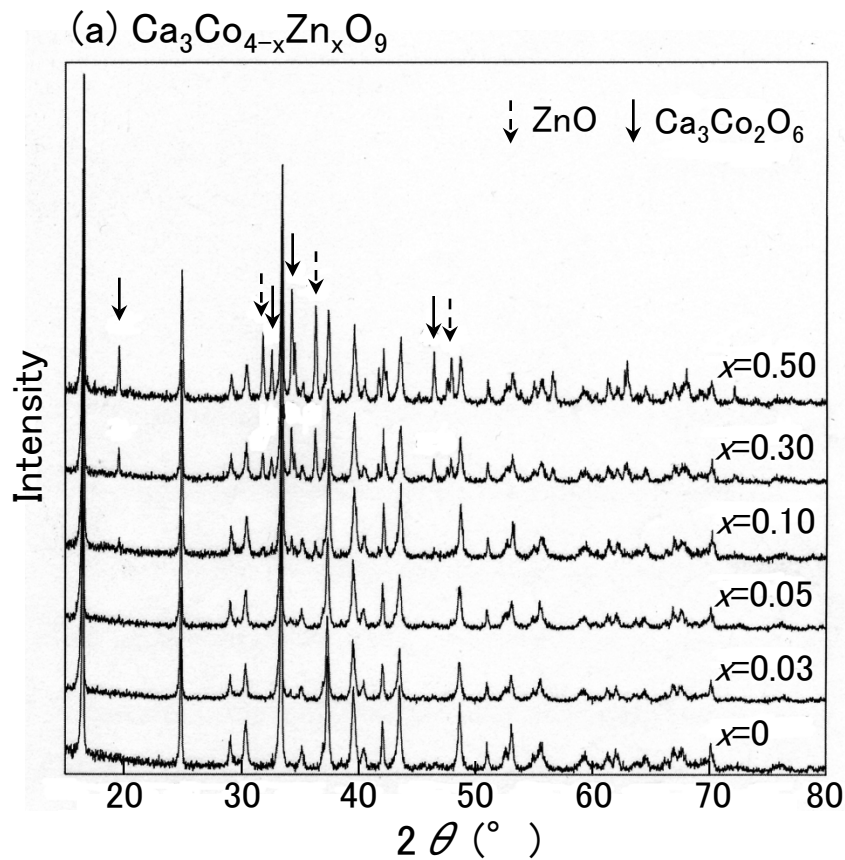


Fig.1

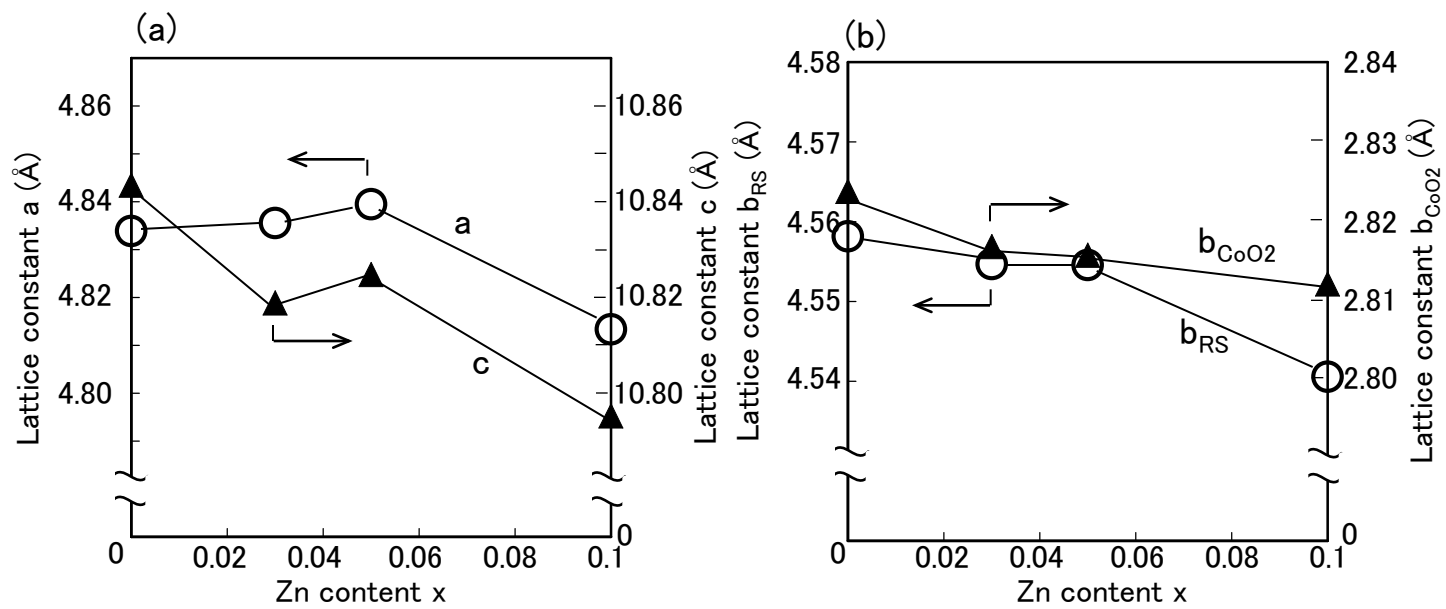


Fig.2

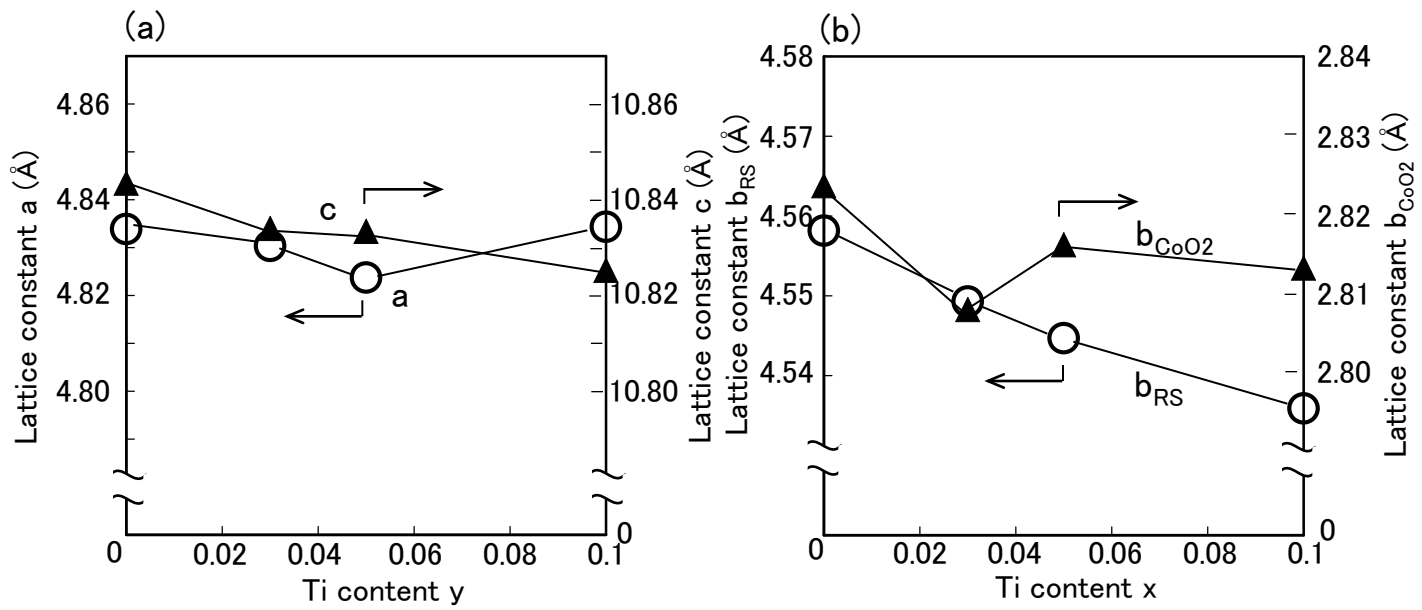


Fig.3

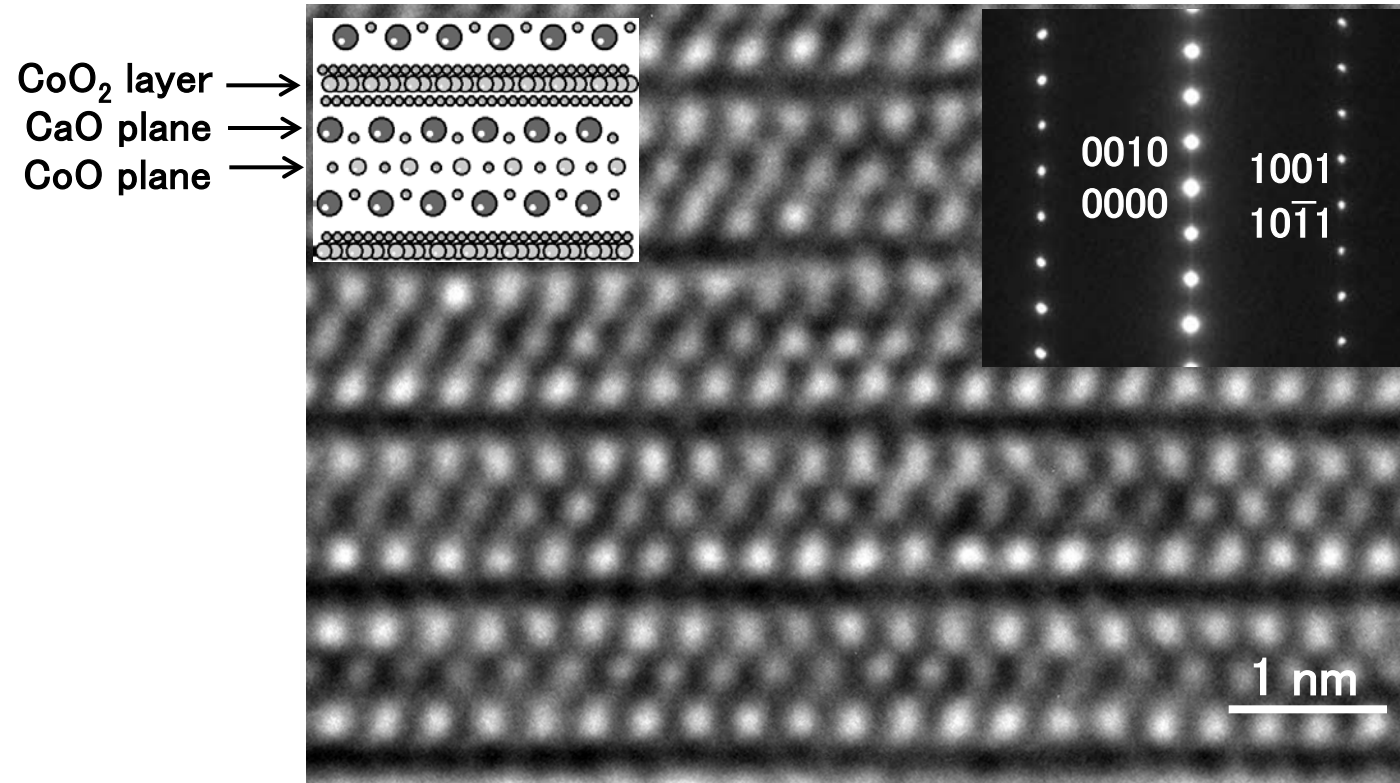


Fig.4

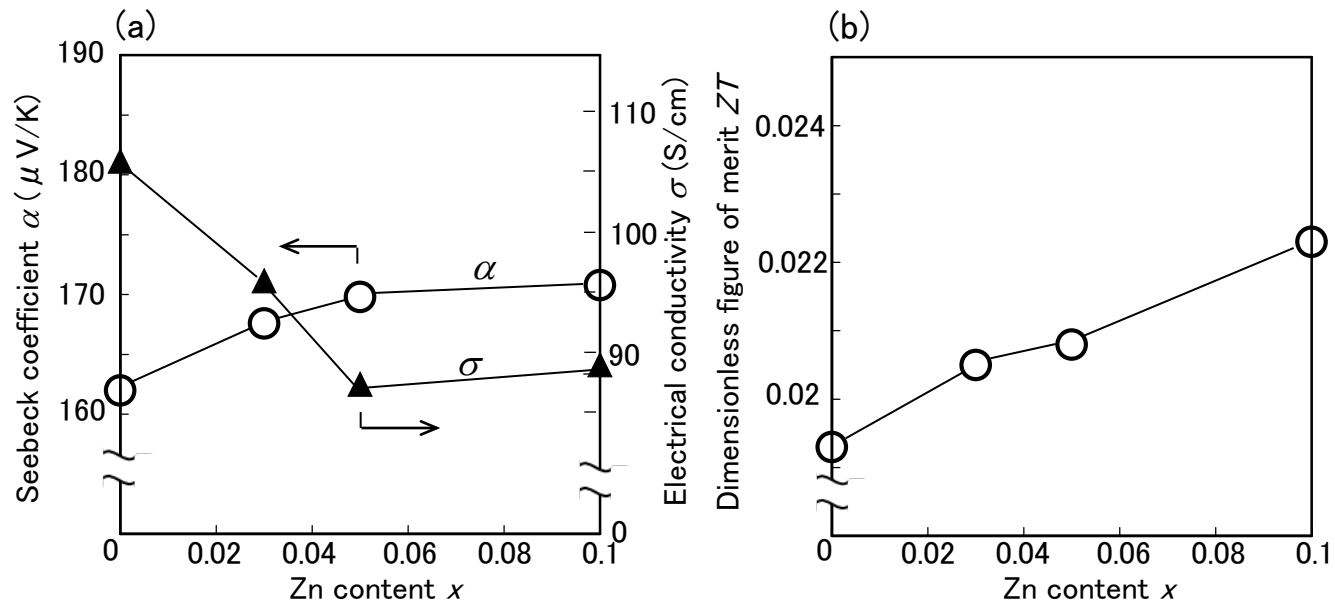


Fig.5

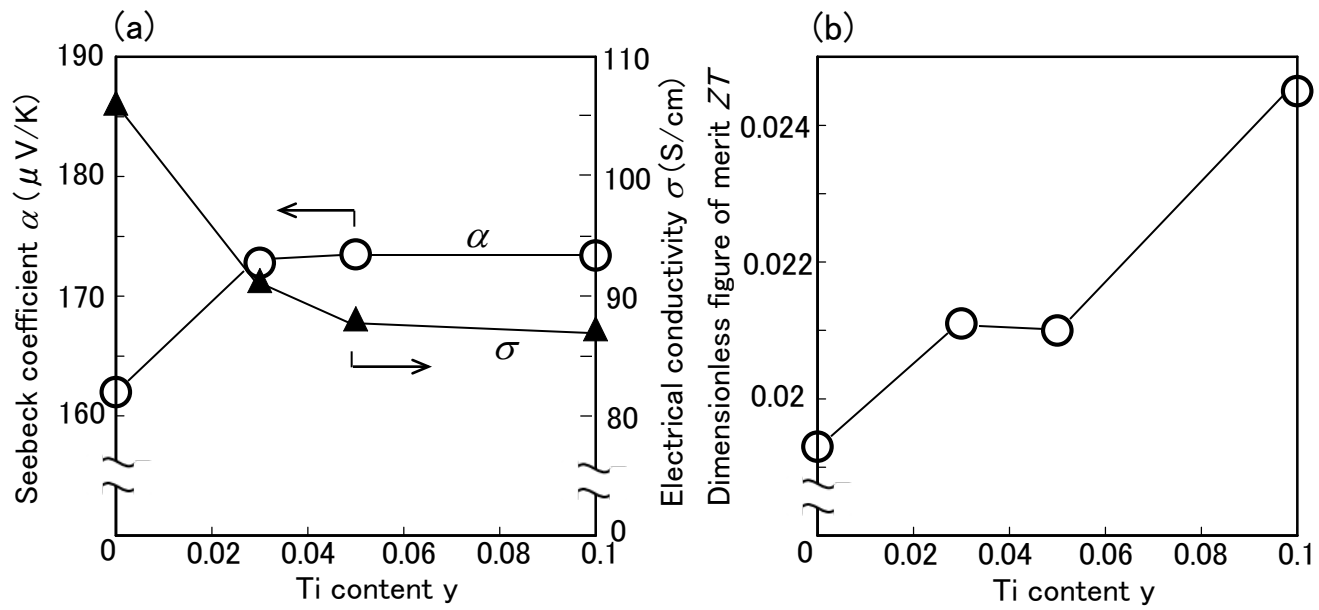


Fig.6

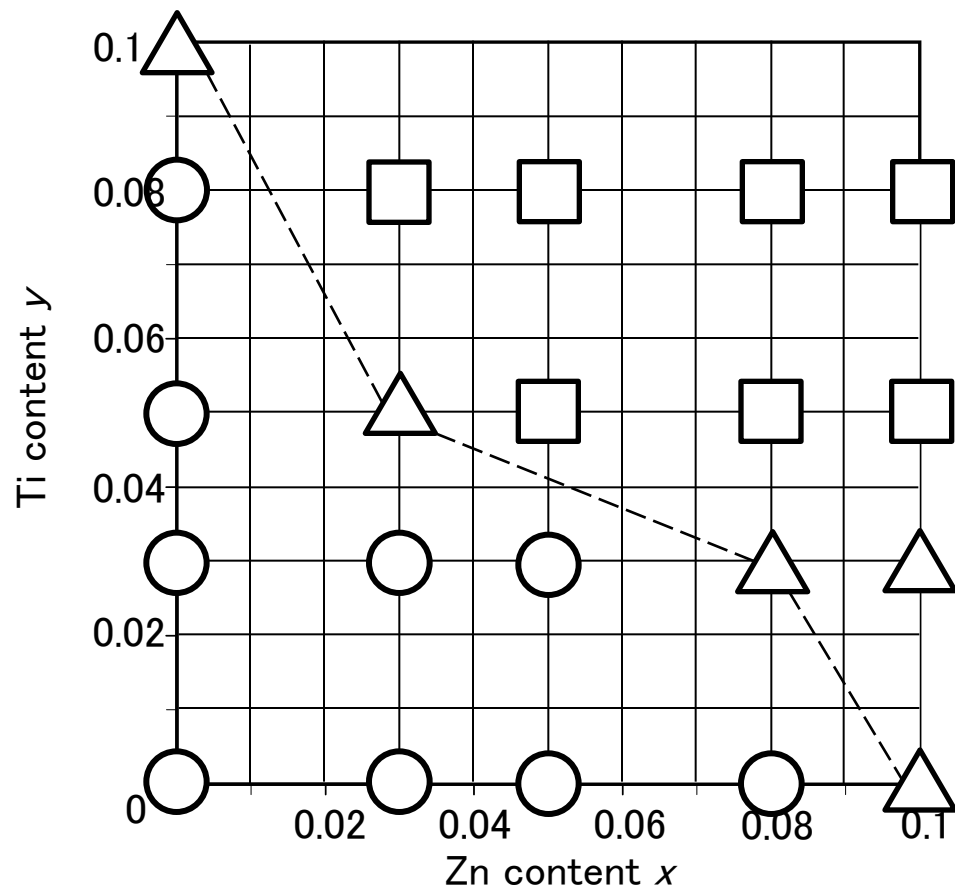


Fig.7

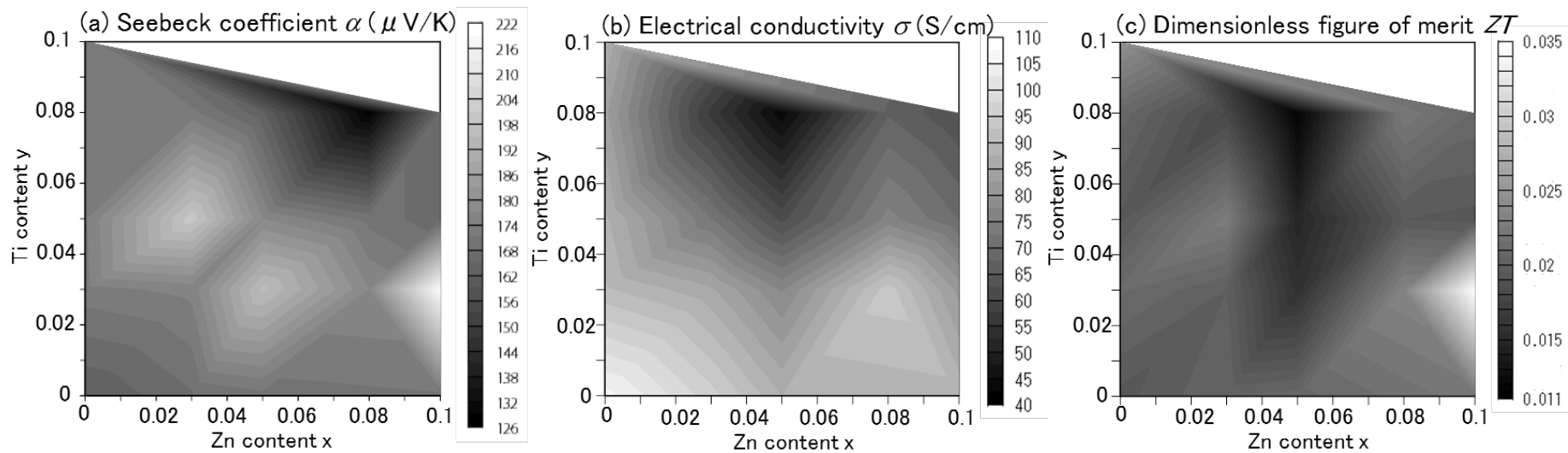


Fig.8